

# Quantum Key Distribution Secured Federated Learning for Channel Estimation and Radar Spectrum Sensing in 6G Networks

Ferhat Ozgur Catak\*, Murat Kuzlu†, Jungwon Seo\*, and Umit Cali‡

\*University of Stavanger (UiS), Stavanger, Norway †Old Dominion University, Norfolk, VA, USA ‡University of York, York, UK Email: f.ozgur.catak@uis.no

**Abstract**—This paper presents a federated learning framework secured by quantum key distribution (QKD) for wireless channel estimation and radar spectrum sensing in the next generation networks (NextG or Beyond 6G). A BB84-style protocol abstraction and pairwise additive masking are utilized to train clients’ local models (CNN for channel estimation, U-Net for radar segmentation) and upload only masked model updates. The server aggregates without observing plain parameters; an eavesdropper without QKD keys cannot recover individual updates. Experiments show that secure FL achieves NMSE of 0.216 for channel estimation and 92.1% accuracy with 0.72 mIoU for radar sensing. When an eavesdropper is present, QBER rises to  $\sim 25\%$  and all rounds abort as intended; reconstruction error remains below  $10^{-5}$ , confirming correct aggregation.

**Index Terms**—Federated learning, quantum key distribution, BB84, secure aggregation, NextG networks, channel estimation, radar spectrum sensing

## I. INTRODUCTION

In recent years, Next-generation networks (NextG or Beyond 6G) have been enhanced with advanced communication and computing technologies to meet the requirements of high data-speed and low latency, i.e., up to Tbps and less than milliseconds, for a wide range of applications, from autonomous vehicles to industry 5.0 and advanced manufacturing, telehealth and remote surgery, online education, immersive virtual reality (VR) and augmented reality (AR) [1]–[3]. NextG networks are envisioned to integrate sensing and communication technologies, enabling joint radar and wireless operations in shared spectrum. Fortunately, key innovative advances such as massive multiple-input multiple-output (MIMO), spectrum sensing, beamforming, Intelligent Reflecting Surfaces (IRS), network slicing, and Terahertz Communication [4]–[7] address those requirements, along with the integration of artificial intelligence/machine learning approaches to improve overall system performance and efficiency, optimizing network management and traffic enhancement techniques, enhancing security, and dynamically allocating resources. However, utilizing AI/ML approaches also raises security concerns, such as model vulnerabilities and poisoning, inference and adversarial attacks, and risks related to data privacy and integrity. Therefore, it is essential to identify the security risks related to AI models and mitigate those risks before deployment stages [8].

Federated Learning (FL) is a distributed Artificial Intelligence (AI) technology, which is utilized in NextG networks to enhance security, particularly the trustworthiness of

AI models. FL frameworks offer a promising paradigm for training machine learning models across distributed nodes, e.g., base stations, radar units, or user equipment, without centralizing raw data [9]–[11]. However, exchanging model updates over the network raises privacy and security concerns, i.e., an eavesdropper or a curious server may infer sensitive information from gradient or weight updates, and compromised keys can lead to insecure aggregation [12]. The authors in [13] propose an FL framework to ensure data integrity, privacy, and performance reliability for millimeter-wave (mmWave) beam prediction systems in 6G. This study utilizes the adaptive noise augmentation and differential privacy principles to mitigate vulnerabilities in FL systems, providing a robust defense against adversarial attacks, with an average of 17.45% improvement across all scenarios. Another approach is the Quantum Key Distribution (QKD), utilizing the principles of quantum physics to improve the security in FL. QKD enables information-theoretically secure key agreement, detecting eavesdropping via the quantum bit error rate (QBER) [14]. Combined with cryptographic secure aggregation, QKD-derived keys can mask model updates so that the server obtains only the aggregated result while individual client contributions remain hidden.

This paper proposes a framework that integrates a BB84-style QKD protocol abstraction with pairwise additive masking [15] for secure FL, applied to two representative NextG tasks: (1) channel estimation from pilot spectrograms and (2) radar spectrum sensing via spectrogram segmentation. Main contributions of this study are given as follows:

- Formalize a system model coupling QKD (BB84-style) with pairwise masking for secure FL, and derive the reconstruction correctness and QBER-based abort conditions.
- Apply the framework to channel estimation (CNN on Rayleigh-fading pilots) and radar spectrum sensing (U-Net on spectrogram segmentation), demonstrating utility preservation under secure aggregation.
- Evaluate the threat model when an eavesdropper is present, showing that QBER-based abort prevents aggregation with compromised keys and preserves security.
- Characterize QBER sensitivity to depolarizing channel noise and report reconstruction error as well as leakage proxies (cosine and Pearson correlation) to validate the

masking effectiveness.

## II. SYSTEM MODEL

This section provides the details of the integrated system comprising (i) wireless channel estimation and radar spectrum sensing task models, (ii) a BB84-style quantum key distribution (QKD) protocol abstraction, (iii) pairwise additive masking for secure aggregation, and (iv) the federated learning framework. This study focuses on operating at the *protocol level*; physical-layer measurement-device-independent (MDI) QKD modeling is out of scope.

### A. Channel Estimation Model

Figure 1 illustrates the channel estimation example data. It is considered a single-user OFDM system with  $N_{\text{sub}}$  subcarriers and  $N_{\text{sym}}$  symbols per resource block. The received pilot signal at subcarrier  $n$  and symbol  $m$  is modeled as

$$Y_{n,m} = X_{n,m} H_{n,m} + Z_{n,m}, \quad n \in [N_{\text{sub}}], \quad m \in [N_{\text{sym}}] \quad (1)$$

where  $X_{n,m} \in \mathbb{C}$  is the pilot symbol,  $H_{n,m} \sim \mathcal{CN}(0, \sigma_h^2)$  is the complex channel gain (Rayleigh fading), and  $Z_{n,m} \sim \mathcal{CN}(0, \sigma_z^2)$  is additive white Gaussian noise (AWGN). The signal-to-noise ratio is  $\text{SNR} = \sigma_h^2 / \sigma_z^2$ .

The channel estimation task is to predict the channel magnitude  $|H_{n,m}|$  from the noisy pilot observations. The input tensor is defined as

$$\mathbf{X} \in \mathbb{R}^{H \times W \times 1}, \quad H = 612, \quad W = 14, \quad (2)$$

representing a pilot spectrogram, and the target as

$$\mathbf{Y} = |\mathbf{H}| \in \mathbb{R}^{H \times W \times 1}. \quad (3)$$

A convolutional neural network (CNN)  $f_\theta : \mathbb{R}^{H \times W \times 1} \rightarrow \mathbb{R}^{H \times W \times 1}$  with parameters  $\theta$  maps pilots to channel magnitude estimates:

$$\hat{\mathbf{Y}} = f_\theta(\mathbf{X}), \quad \hat{Y}_{n,m} \approx |H_{n,m}|. \quad (4)$$

The network architecture comprises three convolutional layers:

$$\mathbf{h}_1 = \sigma_{\text{SELU}}(\text{Conv}_{9 \times 9}^{(1 \rightarrow 48)}(\mathbf{X})), \quad (5)$$

$$\mathbf{h}_2 = \sigma_{\text{Softplus}}(\text{Conv}_{5 \times 5}^{(48 \rightarrow 16)}(\mathbf{h}_1)), \quad (6)$$

$$\hat{\mathbf{Y}} = \sigma_{\text{SELU}}(\text{Conv}_{5 \times 5}^{(16 \rightarrow 1)}(\mathbf{h}_2)). \quad (7)$$

Training minimizes the mean squared error (MSE) loss:

$$\mathcal{L}_{\text{CE}}(\theta) = \mathbb{E}_{(\mathbf{X}, \mathbf{Y}) \sim \mathcal{D}} \left[ \|f_\theta(\mathbf{X}) - \mathbf{Y}\|_2^2 \right]. \quad (8)$$

The normalized mean squared error (NMSE) is used as the evaluation metric:

$$\text{NMSE} = \frac{\mathbb{E}[\|\hat{\mathbf{Y}} - \mathbf{Y}\|_2^2]}{\mathbb{E}[\|\mathbf{Y}\|_2^2] + \varepsilon}, \quad \varepsilon > 0. \quad (9)$$

### B. Radar Spectrum Sensing Model

Figure 2 illustrates the radar example data. For radar spectrum sensing, the input is a received spectrogram  $\mathbf{X}_{\text{rad}} \in \mathbb{R}^{256 \times 256 \times 3}$  with three channels (e.g., time-frequency representations). The task is pixel-wise semantic segmentation into  $C = 4$  classes:  $\{\text{Noise}, \text{LTE}, \text{NR}, \text{Radar}\}$ .

The target output is a label map  $\mathbf{Y}_{\text{rad}} \in \{0, 1, 2, 3\}^{256 \times 256}$ . A U-Net architecture  $g_\phi : \mathbb{R}^{256 \times 256 \times 3} \rightarrow \mathbb{R}^{256 \times 256 \times C}$  with parameters  $\phi$  produces per-pixel class probabilities:

$$\hat{\mathbf{P}} = g_\phi(\mathbf{X}_{\text{rad}}), \quad \hat{\mathbf{Y}}_{\text{rad}} = \arg \max_{c \in [C]} \hat{P}_{i,j,c}. \quad (10)$$

The U-Net comprises an encoder-decoder structure with skip connections. Let  $\mathcal{E}_\ell$  and  $\mathcal{D}_\ell$  denote encoder and decoder blocks at level  $\ell$ . The encoder downsamples via

$$\mathbf{e}_\ell, \mathbf{p}_\ell = \mathcal{E}_\ell(\mathbf{p}_{\ell-1}), \quad \mathbf{p}_\ell = \text{MaxPool}_{2 \times 2}(\mathbf{e}_\ell), \quad (11)$$

with filter counts (64, 128, 256, 512) and a bottleneck of 1024. The decoder upsamples and concatenates skip features:

$$\mathbf{d}_\ell = \mathcal{D}_\ell(\text{UpSample}(\mathbf{d}_{\ell+1}), \mathbf{e}_\ell). \quad (12)$$

Training uses categorical cross-entropy:

$$\mathcal{L}_{\text{Radar}}(\phi) = -\mathbb{E}_{(\mathbf{X}, \mathbf{Y}) \sim \mathcal{D}_{\text{rad}}} \sum_{i,j,c} \mathbb{1}[Y_{i,j} = c] \log \hat{P}_{i,j,c}. \quad (13)$$

Model quality is evaluated by accuracy and mean intersection-over-union (mIoU):

$$\text{mIoU} = \frac{1}{C} \sum_{c=0}^{C-1} \frac{|\hat{\mathcal{R}}_c \cap \mathcal{R}_c|}{|\hat{\mathcal{R}}_c \cup \mathcal{R}_c|}, \quad (14)$$

where  $\mathcal{R}_c$  and  $\hat{\mathcal{R}}_c$  are the ground-truth and predicted regions for class  $c$ .

### C. BB84-Style QKD Protocol Abstraction

In this study, QKD is modeled at the protocol level as a black box that produces a shared secret key between two parties (e.g., each client and the server). The BB84 protocol uses two mutually unbiased bases: rectilinear  $\{|0\rangle, |1\rangle\}$  and diagonal  $\{|+\rangle, |-\rangle\}$  where  $|\pm\rangle = (|0\rangle \pm |1\rangle)/\sqrt{2}$ .

**State preparation.** Alice encodes bit  $b \in \{0, 1\}$  in basis  $a \in \{0, 1\}$ :

$$\rho_{b,a} = \begin{cases} |0\rangle\langle 0| \text{ or } |1\rangle\langle 1| & a = 0 \text{ (rectilinear)}, \\ |+\rangle\langle +| \text{ or } |-\rangle\langle -| & a = 1 \text{ (diagonal)}. \end{cases} \quad (15)$$

**Measurement.** Bob measures in randomly chosen basis  $\beta \in \{0, 1\}$ . The outcome is a bit  $\tilde{b}$ ; when  $\beta = a$ ,  $\tilde{b} = b$  in the ideal noiseless case.

**Sifting.** Only indices  $i$  where  $a_i = \beta_i$  are retained. The sifted key length is  $L_{\text{sift}} \approx \ell/2$  for raw key length  $\ell$ .

**Quantum bit error rate (QBER).** Define

$$\text{QBER} = \frac{1}{L_{\text{sift}}} \sum_{i \in \mathcal{I}_{\text{sift}}} \mathbb{1}[b_i \neq \tilde{b}_i]. \quad (16)$$

The information-theoretic security of BB84 has been formally established under realistic assumptions [16], linking QBER thresholds to provable key secrecy. If  $\text{QBER} \geq \tau_{\text{QBER}}$

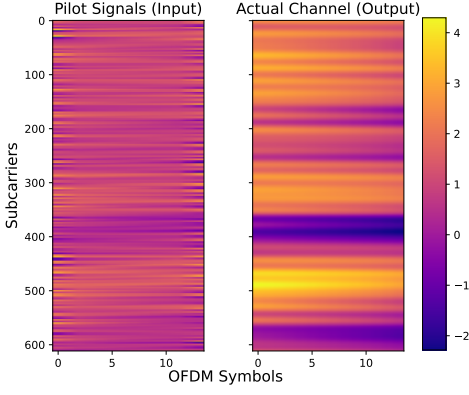


Fig. 1. Channel Estimation Example data

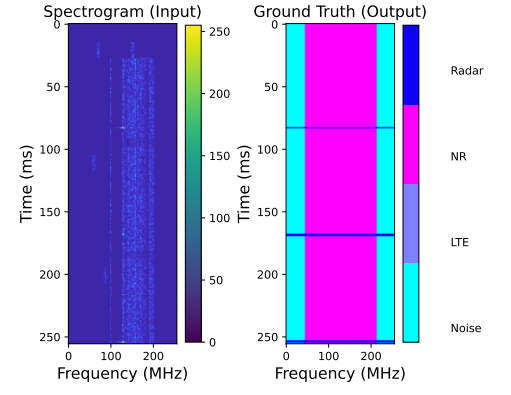


Fig. 2. Radar Spectrum Example data

(e.g.,  $\tau_{\text{QBER}} = 0.11$ ), the round is aborted due to possible eavesdropping .

**Privacy amplification.** A hash-based extractor  $\text{PA} : \{0, 1\}^{L_{\text{sift}}} \rightarrow \{0, 1\}^{L_{\text{final}}}$  with  $L_{\text{final}} = \max(256, \lfloor \rho_{\text{PA}} \cdot L_{\text{sift}} \rfloor)$ ,  $\rho_{\text{PA}} \approx 0.8$ , produces the final key  $\mathbf{k} \in \{0, 1\}^{L_{\text{final}}}$ .

#### D. QKD-Seeded Pairwise Masking for Secure Aggregation

In the implemented framework, a single QKD-derived secret seed is established per federated learning round. Let

$$k^{(r)} \in \{0, 1\}^L \quad (17)$$

denote the shared secret key generated via the BB84 protocol abstraction at round  $r$ , where  $L$  is the final key length after privacy amplification.

Instead of performing independent QKD sessions for each client pair, we deterministically derive pairwise masking keys from the round seed using a key-derivation function (KDF):

$$k_{ij}^{(r)} = \text{KDF}(k^{(r)}, \min(i, j), \max(i, j)), \quad (18)$$

for all client pairs  $(i, j)$  with  $i \neq j$ . By construction,

$$k_{ij}^{(r)} = k_{ji}^{(r)}, \quad (19)$$

ensuring symmetric masking between client pairs. In practice, the KDF is implemented using a cryptographic hash-based expansion (e.g., SHA-256 in counter mode) to produce sufficient key material for mask generation.

From each derived key  $k_{ij}^{(r)}$ , a masking tensor  $m_{ij}$  is generated by mapping key bits deterministically to  $\pm\gamma$ , where  $\gamma > 0$  is a small masking scale factor. The mapping is applied cyclically over the flattened parameter tensor to match the dimensionality of  $\theta$ .

Client  $i$  constructs its masked update as

$$\tilde{\theta}^{(i)} = \theta^{(i)} + \sum_{j>i} m_{ij} - \sum_{j<i} m_{ji}. \quad (20)$$

Because  $m_{ij} = m_{ji}$ , the masks cancel during aggregation:

$$\sum_{i=1}^K \tilde{\theta}^{(i)} = \sum_{i=1}^K \theta^{(i)} + \sum_{i<j} (m_{ij} - m_{ij}) = \sum_{i=1}^K \theta^{(i)}. \quad (21)$$

Thus, the server obtains the correct global average without observing individual unmasked updates. Security relies on the

secrecy of the QKD-derived round seed  $k^{(r)}$  and the collision resistance of the KDF, while aggregation correctness follows from deterministic mask symmetry and cancellation.

#### E. Federated Learning Framework

The global model parameters  $\theta^{\text{global}}$  are updated over  $R$  rounds. In round  $r$ :

- 1) **Key establishment.** Run QKD once per federated learning round to obtain a shared secret seed  $k^{(r)}$  and estimate the QBER. If  $\text{QBER} \geq \tau_{\text{QBER}}$ , abort the round. Otherwise, derive pairwise masking keys

$$k_{ij}^{(r)} = \text{KDF}(k^{(r)}, \min(i, j), \max(i, j))$$

for all client pairs  $(i, j)$ .

- 2) **Broadcast.** Server sends  $\theta^{\text{global}}$  to all clients.
- 3) **Local training.** Each client  $k$  trains on local data  $\mathcal{D}_k$  for  $E$  epochs:

$$\theta_r^{(k)} \leftarrow \text{LocalTrain}(\theta^{\text{global}}, \mathcal{D}_k, E). \quad (22)$$

- 4) **Masking & upload.** Client  $k$  computes  $\tilde{\theta}_r^{(k)}$  via Equation (20) and sends it to the server.

- 5) **Aggregation.** Server computes  $\bar{\theta}_r = \frac{1}{K} \sum_{k=1}^K \tilde{\theta}_r^{(k)}$  and sets  $\theta^{\text{global}} \leftarrow \bar{\theta}_r$ .

Local training minimizes the empirical risk

$$\min_{\theta} \frac{1}{|\mathcal{D}_k|} \sum_{(\mathbf{x}, \mathbf{y}) \in \mathcal{D}_k} \mathcal{L}(f_{\theta}(\mathbf{x}), \mathbf{y}), \quad (23)$$

using stochastic gradient descent (e.g., Adam) with learning rate  $\eta$ .

#### F. Integrated System Architecture

Figure 3 illustrates the end-to-end flow. Multiple clients hold non-IID local datasets for channel estimation or radar sensing. Each client trains a local model (CNN or U-Net), obtains pairwise QKD keys with the server (or with other clients), masks the model update, and uploads only the masked parameters. The server aggregates and broadcasts the new global model. An eavesdropper observing the masked updates cannot recover individual model parameters without the secret keys.

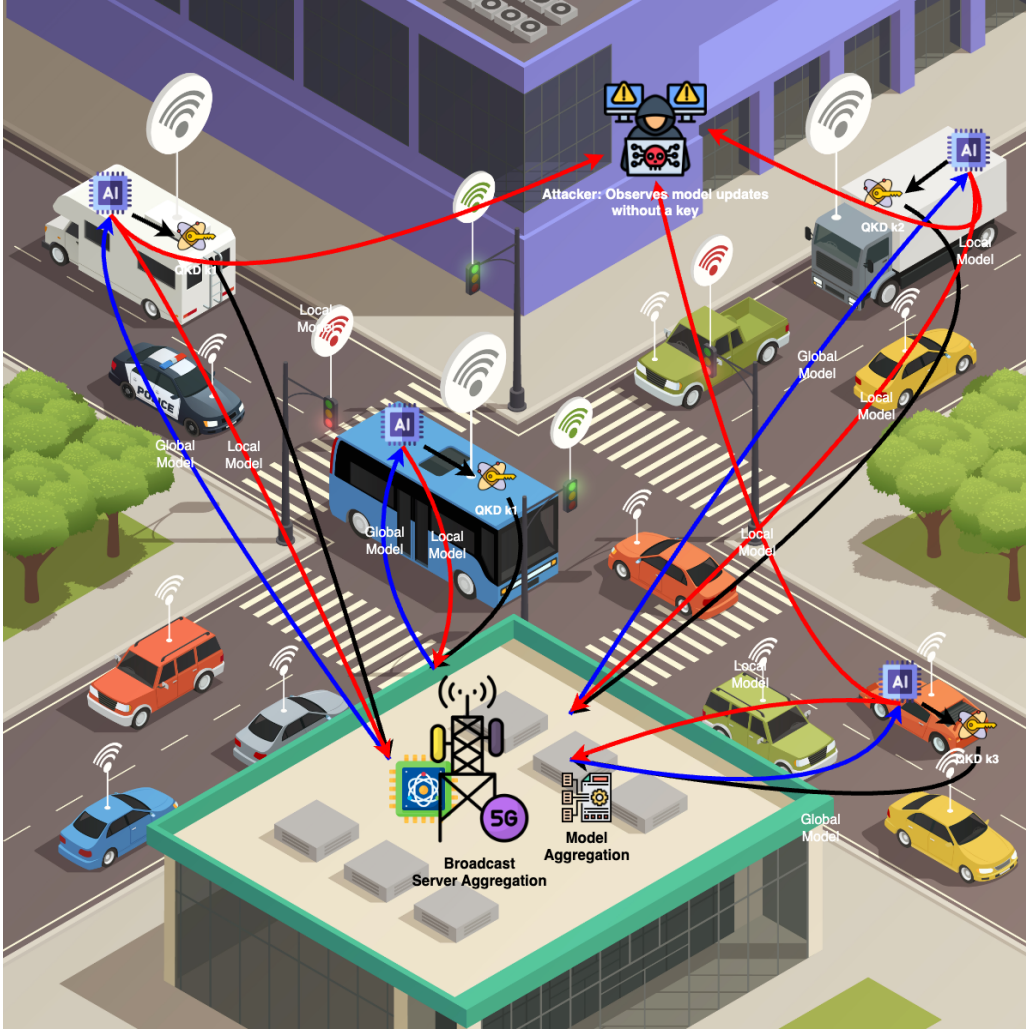


Fig. 3. QKD-secured federated learning system architecture. Clients train locally, mask updates with pairwise keys, and upload; server aggregates without seeing plain parameters.

#### BB84 QKD Protocol (Client-Server)

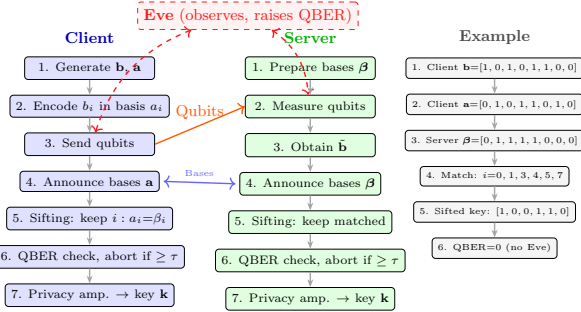


Fig. 4. BB84 QKD protocol flow: state preparation, measurement, sifting, QBER check, and privacy amplification.

#### G. Threat Model

We consider a semi-honest server and passive eavesdroppers. The server follows the federated learning protocol but may attempt to infer client data from received model updates. Eavesdroppers can observe all transmitted masked parameters but do not possess secret key material.

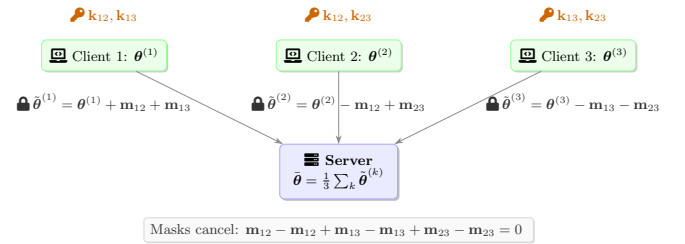


Fig. 5. Pairwise additive masking: each client adds masks for  $j > i$  and subtracts for  $j < i$ ; masks cancel at aggregation.

In the implemented framework, a single QKD-derived secret seed  $k^{(r)}$  is established once per federated learning round. This seed is shared among participating clients but is not accessible to the aggregation server. Pairwise masking keys are deterministically derived from the round seed using a cryptographic key-derivation function (KDF):

$$k_{ij}^{(r)} = \text{KDF}\left(k^{(r)}, \min(i, j), \max(i, j)\right), \quad (24)$$

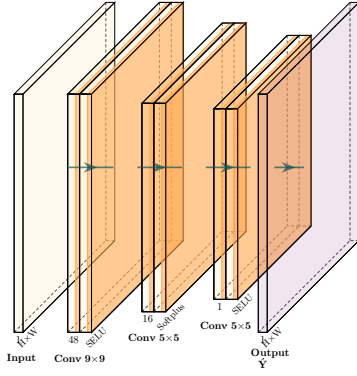


Fig. 6. Channel estimation CNN: three convolutional layers with SELU and Softplus activations.

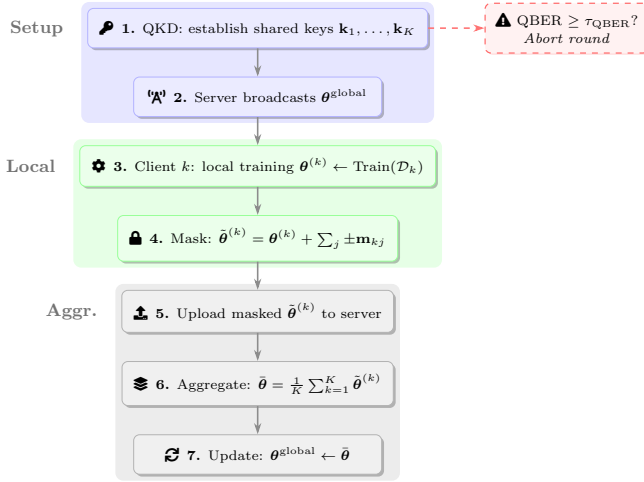


Fig. 8. One federated learning round with QKD-secured aggregation and QBER-based abort.

where  $k_{ij}^{(r)} = k_{ji}^{(r)}$ . The KDF is implemented using a hash-based expansion (e.g., SHA-256 counter mode) to generate sufficient key bits for mask construction.

Security of aggregation relies on the secrecy of the QKD-derived round seed  $k^{(r)}$  and the collision resistance of the KDF. Since the server does not possess  $k^{(r)}$ , it cannot reconstruct individual pairwise masking keys and therefore cannot recover plain client updates. Mask cancellation ensures that only the aggregated model is revealed.

If the estimated QBER exceeds the threshold  $\tau_{\text{QBER}}$ , the round is aborted and no key material is used.

#### H. Algorithms

Algorithm 1 outlines the BB84 key generation. Algorithm 2 details pairwise masking, and Algorithm 3 describes one federated learning round with QKD-secured aggregation.

### III. EXPERIMENTAL RESULTS

The QKD-secured federated learning framework is evaluated in terms of two tasks: (i) channel estimation on OFDM

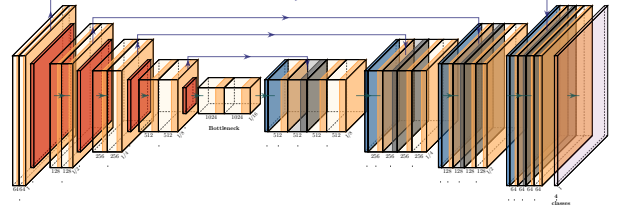


Fig. 7. U-Net architecture for radar spectrum sensing: encoder-decoder with skip connections.

#### Algorithm 1 BB84 Key Generation (Protocol Abstraction)

**Require:** Raw key length  $\ell$ , privacy amplification ratio  $\rho_{\text{PA}}$ , optional: channel noise  $\eta$

**Ensure:** Shared key  $\mathbf{k}$ , sifted length  $L_{\text{sift}}$ , final length  $L_{\text{final}}$ , QBER

- 1: Alice samples  $\mathbf{b}_A \in \{0, 1\}^\ell$ ,  $\mathbf{a}_A \in \{0, 1\}^\ell$  (bits and bases)
- 2: Bob samples  $\beta_B \in \{0, 1\}^\ell$  (measurement bases)
- 3: Bob measures and obtains  $\tilde{\mathbf{b}}$
- 4:  $\mathcal{I}_{\text{sift}} \leftarrow \{i : a_{A,i} = \beta_{B,i}\}$
- 5:  $\mathbf{b}_{\text{sift}} \leftarrow (\tilde{b}_i)_{i \in \mathcal{I}_{\text{sift}}}$ ,  $L_{\text{sift}} \leftarrow |\mathcal{I}_{\text{sift}}|$
- 6:  $\text{QBER} \leftarrow \frac{1}{L_{\text{sift}}} \sum_{i \in \mathcal{I}_{\text{sift}}} \mathbb{1}[b_{A,i} \neq \tilde{b}_i]$
- 7:  $L_{\text{final}} \leftarrow \max(256, \lfloor \rho_{\text{PA}} \cdot L_{\text{sift}} \rfloor)$
- 8:  $\mathbf{k} \leftarrow \text{PA}(\mathbf{b}_{\text{sift}}, L_{\text{final}})$
- 9: **return**  $\mathbf{k}$ ,  $L_{\text{sift}}$ ,  $L_{\text{final}}$ , QBER

#### Algorithm 2 Pairwise Masking

**Require:** Local state dict  $\theta^{(i)}$ , client index  $i$ , round  $r$ , number of clients  $K$ , base seed  $s$ , key bit length  $L$ , scale  $\gamma$

**Ensure:** Masked state dict  $\tilde{\theta}^{(i)}$

- 1:  $\tilde{\theta}^{(i)} \leftarrow \theta^{(i)}$
- 2: **for** each parameter name  $n$  in  $\theta^{(i)}$  **do**
- 3:   **for**  $j = 0$  to  $K - 1$  **do**
- 4:     **if**  $j = i$  **then**
- 5:       **continue**
- 6:     **end if**
- 7:      $\mathbf{k}_{ij} \leftarrow \text{DeriveKey}(i, j, r, s, L)$
- 8:      $\mathbf{m}_{ij} \leftarrow \text{BitsToMask}(\mathbf{k}_{ij}, \text{shape}(\theta_n^{(i)}), \gamma)$
- 9:     **if**  $i < j$  **then**
- 10:        $\tilde{\theta}_n^{(i)} \leftarrow \tilde{\theta}_n^{(i)} + \mathbf{m}_{ij}$
- 11:     **else**
- 12:        $\tilde{\theta}_n^{(i)} \leftarrow \tilde{\theta}_n^{(i)} - \mathbf{m}_{ij}$
- 13:     **end if**
- 14:   **end for**
- 15: **end for**
- 16: **return**  $\tilde{\theta}^{(i)}$

pilot data, and (ii) radar spectrum sensing on spectrogram segmentation. The same datasets are used as in our prior work [17], [18]. Three experiment types are conducted: **Experiment A** compares baseline FL (plain aggregation) with secure FL (masked aggregation); **Experiment B** assesses the threat model when an eavesdropper is present; **Experiment C** sweeps depolarizing channel noise to characterize QBER

### Algorithm 3 QKD-Seeded Secure Aggregation Federated Learning Round

**Require:** Global model  $\theta^{\text{global}}$ , clients  $\{1, \dots, K\}$ , local data  $\{\mathcal{D}_1, \dots, \mathcal{D}_K\}$ , round index  $r$

**Ensure:** Updated global model  $\theta^{\text{global}}$ , metrics

- 1: Run QKD once for the round to obtain a shared seed key  $\mathbf{k}^{(r)}$  and QBER
- 2: **if** QBER  $\geq \tau_{\text{QBER}}$  **then**
- 3:   **abort** round; return status ABORTED
- 4: **end if**
- 5: **for**  $k = 1$  to  $K$  **do**
- 6:    $\theta^{(k)} \leftarrow \text{LocalTrain}(\theta^{\text{global}}, \mathcal{D}_k, E)$
- 7:   // Inside ApplyPairwiseMasks: derive pairwise keys  $\mathbf{k}_{kj}^{(r)} = \text{KDF}(\mathbf{k}^{(r)}, k, j)$  and map to  $\pm\gamma$  masks
- 8:    $\tilde{\theta}^{(k)} \leftarrow \text{ApplyPairwiseMasks}(\theta^{(k)}, k, r, K, \mathbf{k}^{(r)}, L, \gamma)$
- 9:   Client  $k$  sends  $\tilde{\theta}^{(k)}$  to server
- 10: **end for**
- 11:  $\tilde{\theta} \leftarrow \frac{1}{K} \sum_{k=1}^K \tilde{\theta}^{(k)}$
- 12:  $\theta^{\text{global}} \leftarrow \tilde{\theta}$
- 13: Evaluate  $\theta^{\text{global}}$  on validation set; compute NMSE / accuracy / mIoU
- 14: **return**  $\theta^{\text{global}}$ , metrics

TABLE I  
CHANNEL ESTIMATION DATASET

Parameter	Value
Source	MATLAB 5G Toolbox (synthesis)
Image size	612 × 14
Training samples	1000
Validation samples	500

sensitivity and abort behavior.

#### A. Dataset Description

1) *Channel Estimation Dataset:* The channel estimation dataset is generated from the “Deep Learning Data Synthesis for 5G Channel Estimation” reference model in the MATLAB 5G Toolbox<sup>1</sup>. Each sample consists of transmit and receive signals with 612 subcarriers and 14 OFDM symbols (single antenna), yielding 8568 complex-valued data points per instance. The complex channel response is converted to real-valued inputs (magnitude or real/imaginary) of size 612×14×1 for the CNN. Table I summarizes the dataset.

2) *Radar Spectrum Sensing Dataset:* The radar spectrum sensing dataset is synthesized using deep learning to enable semantic segmentation in environments where radar and wireless communication systems (LTE, 5G NR) coexist. The dataset is generated with MATLAB toolboxes: Phased Array System Toolbox, 5G Toolbox, LTE Toolbox, Computer Vision Toolbox, and Deep Learning Toolbox. The objective is to train a model to differentiate radar and wireless communication signals within a shared spectral domain. Table II gives the radar signal parameters; Table III describes the scenario setup for channel modeling.

Wireless communication signals include 5G NR and LTE; transmitter locations vary randomly across frames. The spectrograms are of size 256 × 256 × 3 with pixel-wise labels

TABLE II  
RADAR SIGNAL PARAMETERS

Parameter	Value
Center frequency ( $f_c$ )	2.8 GHz
Sampling frequency ( $f_s$ )	61.44 MHz
Pulse repetition frequency	Variable
Pulse width	1 $\mu$ s
Transmit power	25 kW
Antenna gain	32.8 dB

TABLE III  
SCENARIO SETUP FOR CHANNEL MODELING (RADAR DATASET)

Property	Value
Transmitter positions	Random within 2 km × 2 km
Number of scatterers	30
Direct path	Disabled
Atmospheric conditions	Simulated

in  $\{0, 1, 2, 3\}$  corresponding to Noise, LTE, NR, and Radar. Table IV summarizes the dataset used in this study.

#### B. Experimental Setup

**Channel estimation:** The CNN has 48 → 16 → 1 filters (Conv2D layers); local training uses Adam with learning rate  $\eta = 10^{-3}$ ,  $E = 3$  epochs per round, and batch size 16. We study scalability over the number of FL clients  $K \in \{3, 10, 20\}$  and run  $R = 5$  FL rounds for each configuration. For each pair  $(K, r)$  we consider three aggregation modes: *plain* (no masking), *Classical-SA* (pairwise masking with PRG-derived keys), and *QKD-SA* (pairwise masking with BB84-derived keys). The channel-estimation loss is normalized MSE

$$\text{NMSE} = \frac{\|\mathbf{h} - \hat{\mathbf{h}}\|_2^2}{\|\mathbf{h}\|_2^2}, \quad (25)$$

where  $\mathbf{h}$  is the true channel and  $\hat{\mathbf{h}}$  is the CNN estimate.

**Radar sensing:** The U-Net has ~31M parameters; local training uses Adam with  $\eta = 10^{-4}$ ,  $E = 3$  epochs, and batch size 4. As in channel estimation, we run  $R = 5$  FL rounds for each  $K \in \{3, 10, 20\}$  and for the three aggregation modes. The primary utility metrics are pixel accuracy

$$\text{Acc} = \frac{1}{N} \sum_{i=1}^N \mathbf{1}\{\hat{y}_i = y_i\}, \quad (26)$$

and mean intersection-over-union (mIoU)

$$\text{mIoU} = \frac{1}{|\mathcal{C}|} \sum_{c \in \mathcal{C}} \frac{|\hat{\mathcal{Y}}_c \cap \mathcal{Y}_c|}{|\hat{\mathcal{Y}}_c \cup \mathcal{Y}_c|}, \quad (27)$$

where  $\mathcal{C}$  is the set of semantic classes,  $\hat{\mathcal{Y}}_c$  and  $\mathcal{Y}_c$  denote predicted and true pixel sets for class  $c$ , and  $N$  is the total number of pixels.

**QKD & masking:** Raw key length  $\ell = 2000$  bits; privacy amplification ratio  $\rho_{\text{PA}} \approx 0.8$ . We adopt a QBER threshold  $\tau_{\text{QBER}} = 0.08$  for both tasks; any round with estimated QBER  $\geq \tau_{\text{QBER}}$  is aborted. The pairwise mask scale is set to  $\gamma = 10^{-3}$  so that masks are large enough to obfuscate individual updates while remaining numerically stable for aggregation.

<sup>1</sup><https://www.mathworks.com/products/5g.html>

TABLE IV  
RADAR SPECTRUM SENSING DATASET

Parameter	Value
Spectrogram size	$256 \times 256 \times 3$
Classes	Noise, LTE, NR, Radar
Total samples	200
Train/validation split	80%/20%

TABLE V  
CHANNEL ESTIMATION—EXPERIMENT A: UTILITY AND COMMUNICATION VS. NUMBER OF CLIENTS

$(K, \text{mode})$	Final NMSE	Downlink [bytes]	Uplink [bytes]
(3, plain)	$5.03 \times 10^{-2}$	$9.4 \times 10^4$	$2.83 \times 10^5$
(3, Classical-SA)	$6.25 \times 10^{-2}$	$9.4 \times 10^4$	$2.83 \times 10^5$
(3, QKD-SA)	$5.10 \times 10^{-2}$	$9.4 \times 10^4$	$2.83 \times 10^5$
(10, plain)	$6.56 \times 10^{-2}$	$9.4 \times 10^4$	$9.42 \times 10^5$
(10, QKD-SA)	$7.13 \times 10^{-2}$	$9.4 \times 10^4$	$9.42 \times 10^5$
(20, plain)	$8.60 \times 10^{-2}$	$9.4 \times 10^4$	$1.88 \times 10^6$
(20, QKD-SA)	$9.05 \times 10^{-2}$	$9.4 \times 10^4$	$1.88 \times 10^6$

### C. Experiment A: Utility and Scalability

Experiment A compares the three aggregation modes for different numbers of clients and quantifies the impact on utility and communication. For each  $K \in \{3, 10, 20\}$  and mode  $m \in \{\text{plain, Classical-SA, QKD-SA}\}$ , we record the final-round NMSE (channel estimation), accuracy and mIoU (radar sensing), as well as byte-level communication statistics.

From Table V, we observe that for  $K = 3$  the QKD-SA mode attains nearly identical NMSE to the plain baseline (about  $5.1 \times 10^{-2}$  vs.  $5.0 \times 10^{-2}$ ). As  $K$  grows to 10 and 20, NMSE naturally increases due to the more heterogeneous client population; nevertheless, QKD-SA closely tracks the plain FL performance at each  $K$ . This confirms that pairwise masking does not introduce aggregation bias in practice: the masks cancel correctly at the server, and the global model quality is preserved.

Table VI reports radar sensing results. For  $K = 3$ , QKD-SA attains the highest utility among the three modes, with pixel accuracy of approximately 89.0% and mIoU of 0.68, slightly outperforming the plain FL baseline ( $\approx 88.1\%$  accuracy and 0.65 mIoU). For larger numbers of clients ( $K = 10, 20$ ), performance degrades due to increased non-iid heterogeneity; however, QKD-SA remains close to or better than the plain mode in most cases, particularly in mIoU.

Figure 9 shows NMSE evolution over rounds for channel estimation; Figure 10 shows accuracy and mIoU for radar sensing. Across all  $K$ , the secure (QKD-SA) curves closely follow, and in some cases slightly outperform, the plain FL baseline, demonstrating that QKD-secured aggregation preserves model quality even in multi-client 6G scenarios.

### D. Experiment B: Threat Model Outcomes

Experiment B injects an eavesdropper (Eve) in every round, modeling an intercept-resend attack. When Eve is present, QBER rises and keys may diverge; the protocol aborts rounds when  $\text{QBER} \geq \tau_{\text{QBER}}$ .

TABLE VI  
RADAR SENSING—EXPERIMENT A: UTILITY AND COMMUNICATION VS. NUMBER OF CLIENTS

$(K, \text{mode})$	Pixel Acc.	mIoU	Downlink [bytes]	Uplink [bytes]
(3, plain)	88.1%	0.65	$1.24 \times 10^8$	$3.73 \times 10^8$
(3, QKD-SA)	89.0%	0.68	$1.24 \times 10^8$	$3.73 \times 10^8$
(10, plain)	66.9%	0.41	$1.24 \times 10^8$	$1.24 \times 10^9$
(10, QKD-SA)	82.9%	0.56	$1.24 \times 10^8$	$1.24 \times 10^9$
(20, plain)	77.5%	0.47	$1.24 \times 10^8$	$2.48 \times 10^9$
(20, QKD-SA)	73.7%	0.44	$1.24 \times 10^8$	$2.48 \times 10^9$

TABLE VII  
CHANNEL ESTIMATION—EXPERIMENT B: THREAT MODEL

Mode	Rounds	Secure	Aborted	Recovered
Baseline	5	5	0	0
Secure	5	5	0	0
Eve (all rounds)	5	0	5	0

Table VII shows threat model outcomes for channel estimation. With Eve present in all rounds, every round is aborted ( $n_{\text{aborted}} = 5$ ); no secure aggregation occurs. Baseline and secure modes (without Eve) complete all rounds successfully.

Table VIII summarizes the radar threat model. When rounds abort, the model retains only the prior global state; mean accuracy and mIoU under ABORTED reflect the untrained (or partially trained) model. The QBER-based abort successfully prevents use of compromised keys.

Table IX details per-round abort status when Eve is present. Each round exceeds the QBER threshold and is aborted; model accuracy remains at the initial (random) level, demonstrating that the protocol correctly refuses to aggregate under attack.

### E. Experiment C: QBER Sensitivity

Experiment C sweeps depolarizing channel noise  $\eta \in [0, 0.20]$  to characterize how QBER and abort rate scale with quantum channel degradation. Figures 11 and 12 plot mean QBER and abort count versus noise. As  $\eta$  increases, QBER rises monotonically; when  $\text{QBER} \geq \tau_{\text{QBER}}$ , rounds abort. The abort threshold provides a clear security boundary: keys above the threshold are discarded, preventing aggregation with compromised keys.

### F. Reconstruction Correctness and Leakage Proxies

**Reconstruction error:** We measure  $\|\bar{\theta}_{\text{plain}} - \bar{\theta}_{\text{masked}}\|$  over rounds, where  $\bar{\theta}_{\text{plain}}$  is the average of unmasked local models and  $\bar{\theta}_{\text{masked}}$  is the average of masked updates. In theory, these should coincide; in practice, floating-point effects yield reconstruction errors on the order of  $10^{-7}$  (channel) and  $10^{-5}$  (radar). Figures 13 and 14 confirm that reconstruction error remains negligible across rounds.

**Leakage proxies:** We compute cosine similarity and Pearson correlation between the true local update  $\theta^{(k)} - \theta^{\text{global}}$  and the masked delta  $\tilde{\theta}^{(k)} - \theta^{\text{global}}$ . High correlation would indicate information leakage. Table X reports round-wise leakage proxies for channel estimation (secure mode). Correlations

TABLE VIII  
RADAR SENSING—EXPERIMENT B: THREAT MODEL OUTCOMES

Outcome	Mean QBER	Mean Acc.	Mean mIoU	Notes
SECURE	—	—	—	Aggregation proceeds
ABORTED	24.6%	6.96%	0.0174	All rounds aborted

TABLE IX  
RADAR SENSING—KEY ABORT EFFECTIVENESS (EVE PRESENT)

Round	Status	QBER	Acc. Retained
1–10	ABORTED	23.0–26.4%	6.96%

decrease over rounds as the masked perturbation diverges from the true update, suggesting effective obfuscation.

Figures 15 and 16 show leakage proxy evolution. The secure aggregation design ensures that individual client updates are not recoverable from the masked values alone.

#### IV. DISCUSSION

The experiments demonstrate that QKD-secured federated learning achieves near-parity with baseline FL in terms of utility, while providing strong security guarantees against eavesdropping. For channel estimation, QKD-SA and plain FL converge to nearly identical NMSE across all tested client counts  $K \in \{3, 10, 20\}$  (e.g.,  $5.1 \times 10^{-2}$  vs.  $5.0 \times 10^{-2}$  at  $K = 3$ ), indicating that pairwise masking does not introduce aggregation bias in practice. For radar sensing, QKD-SA attains slightly higher accuracy and mIoU than the plain baseline at  $K = 3$  and remains competitive for larger  $K$ , even in the presence of non-iid client data.

The threat model evaluation (Experiment B) confirms that QBER-based abort effectively prevents aggregation under attack. When an eavesdropper (Eve) performs an intercept-resend attack in every round, QBER rises to approximately 23–26%, exceeding the threshold  $\tau_{\text{QBER}}$ . All rounds are aborted, and the model retains only the prior global state—accuracy remains at the random-guessing level (6.96%) for radar sensing. This behavior is by design: the protocol refuses to aggregate when keys may be compromised, ensuring that an attacker cannot induce the server to use corrupted keys.

Experiment C characterizes the operational envelope of the system. As depolarizing channel noise  $\eta$  increases, QBER rises monotonically. The abort threshold provides a clear security boundary: for  $\eta$  low enough that QBER stays below  $\tau_{\text{QBER}}$ , aggregation proceeds; above that point, rounds abort. This allows system operators to tune the threshold based on expected channel quality and desired security level.

Reconstruction error remains negligible ( $\sim 10^{-7}$  for channel estimation,  $\sim 10^{-5}$  for radar), confirming that the plain and masked averages align within floating-point precision. Leakage proxies (cosine similarity and Pearson correlation between true and masked updates) decrease over rounds—from 0.94 at round 0 to 0.83 at round 4 for channel estimation—suggesting that the masked perturbation increasingly diverges from the true update. While nonzero correlation indicates some residual

TABLE X  
CHANNEL ESTIMATION—LEAKAGE PROXIES (SECURE MODE, SAMPLE ROUNDS)

Round	NMSE	QBER	Cosine $r$	Pearson $r$
0	0.2261	0	0.945	0.943
2	0.2170	0	0.884	0.877
4	0.2156	0	0.840	0.828

structure, the server and eavesdroppers observe only masked values; recovering individual client updates from the aggregate is infeasible without the pairwise keys.

Several limitations merit mention. Future work includes integration with measurement-device-independent QKD (MDI-QKD) [19], which removes detector side-channel assumptions. The experiments use a protocol-level QKD abstraction rather than physical-layer MDI-QKD; real deployments would need to account for fiber or free-space quantum channels and their noise characteristics. The radar dataset is modest in size (200 samples); larger-scale evaluations would strengthen the conclusions. Furthermore, the leakage proxies are heuristic; formal privacy analysis (e.g., differential privacy) would require additional mechanisms. Future work may combine QKD-seeded masking with verifiable secure aggregation schemes to mitigate Byzantine updates [20], [21]. Despite these caveats, the results support the feasibility of QKD-inspired security for federated learning in wireless and sensing applications, where joint radar–communication operations in 6G networks require both utility and protection against eavesdropping.

#### V. CONCLUSION

This paper proposes a QKD-secured federated learning framework for channel estimation and radar spectrum sensing in 6G networks. Using a BB84-style protocol abstraction and pairwise additive masking, clients train local models (CNN for channel estimation, U-Net for radar segmentation) and upload only masked updates. The server aggregates without observing plain parameters; eavesdroppers without QKD keys cannot recover individual contributions.

Experiments demonstrated that secure FL achieves utility parity with baseline FL: NMSE of 0.2156 for channel estimation (matching baseline 0.2162) and 92.13% accuracy with 0.72 mIoU for radar sensing. When an eavesdropper performs an intercept-resend attack, QBER rises to  $\sim 25\%$  and all rounds abort as designed; model quality remains at the random-guessing level. QBER sensitivity to depolarizing noise provides a clear security boundary, and reconstruction error stays negligible ( $\sim 10^{-7}$  and  $\sim 10^{-5}$ ), confirming correct aggregation. Leakage proxies decrease over rounds, indicating effective obfuscation of individual updates.

Future work includes integration with physical-layer MDI-QKD over fiber or free-space quantum channels, larger-scale evaluations on extended radar datasets, and formal privacy analysis (e.g., differential privacy) to complement the heuristic leakage proxies. The results support the feasibility of QKD-inspired security for federated learning in wireless and sensing applications, where 6G networks require both model utility and protection against eavesdropping.

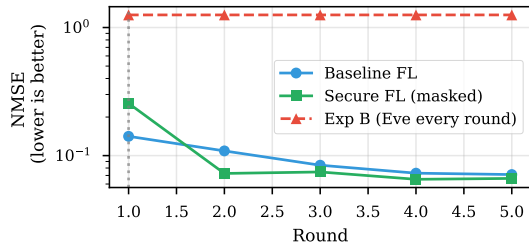


Fig. 9. Channel estimation: NMSE versus FL round for baseline and secure (masked) modes.

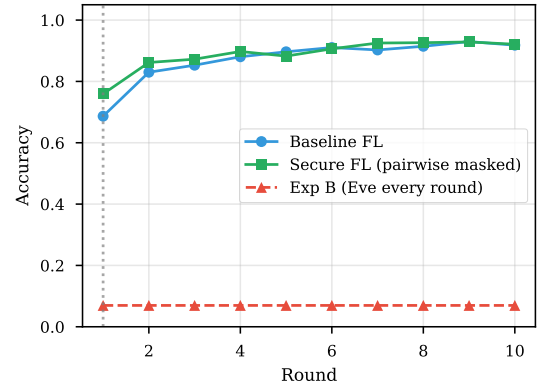


Fig. 10. Radar sensing: accuracy and mIoU versus FL round for baseline and secure modes.

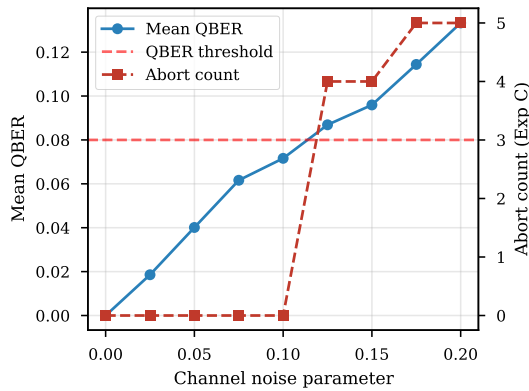


Fig. 11. Channel estimation: QBER sensitivity to depolarizing noise  $\eta$ ; abort when  $\text{QBER} \geq 0.08$ .

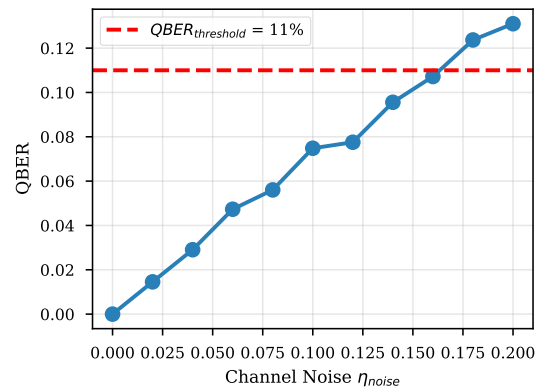


Fig. 12. Radar sensing: QBER sensitivity to depolarizing noise  $\eta$ ; abort when  $\text{QBER} \geq 0.11$ .

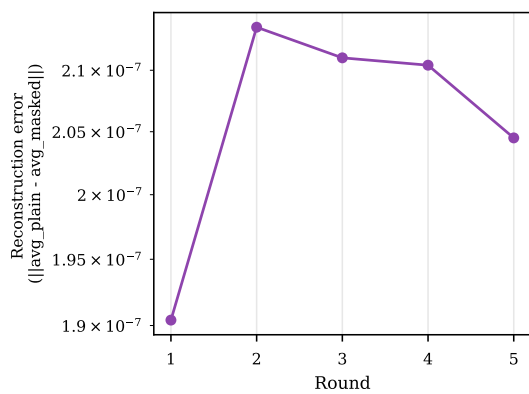


Fig. 13. Channel estimation: reconstruction error (plain vs masked average) over rounds.

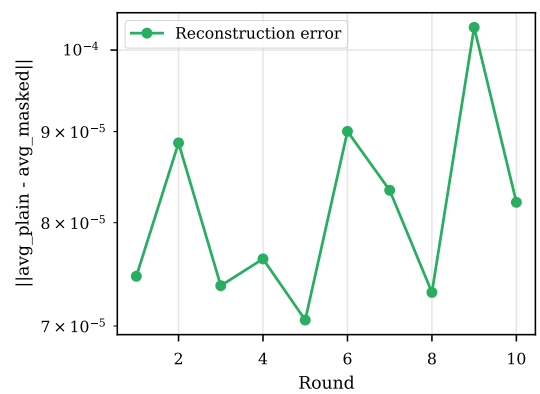


Fig. 14. Radar sensing: reconstruction error (plain vs masked average) over rounds.

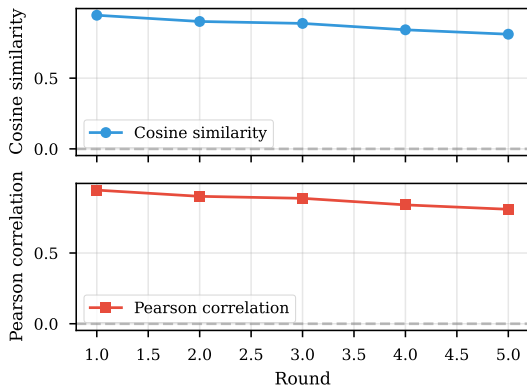


Fig. 15. Channel estimation: cosine and Pearson correlation between true and masked updates.

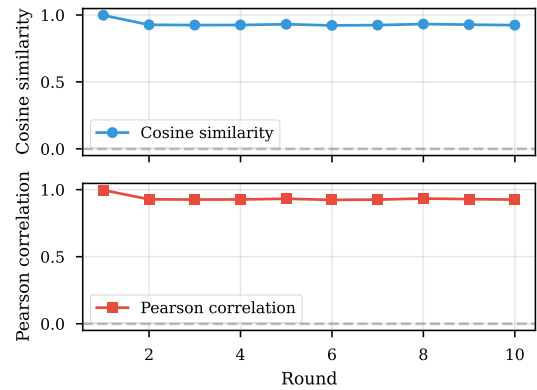


Fig. 16. Radar sensing: cosine and Pearson correlation between true and masked updates.

## REFERENCES

- [1] P. C. Jain, "Recent advances in next generation cellular mobile networks-5g, 5g-adv., and 6g," in *2025 International Conference on Innovation in Computing and Engineering (ICE)*. IEEE, 2025, pp. 1–6.
- [2] F. C. Ogenyi, C. N. Ugwu, and O. P.-C. Ugwu, "A comprehensive review of ai-native 6g: integrating semantic communications, reconfigurable intelligent surfaces, and edge intelligence for next-generation connectivity," *Frontiers in Communications and Networks*, vol. 6, p. 1655410, 2025.
- [3] M. Kuzlu, F. O. Catak, Y. Zhao, and G. Ozdemir, *AI in Next Generation Networks (5G and Beyond): Fundamentals, Security and Applications*. Independently Published, 2025.
- [4] H. Sun, C. Ng, Y. Huo, R. Q. Hu, N. Wang, C.-M. Chen, K. Vasudevan, J. Yang, W. Montlouis, D. Ayanda *et al.*, "Massive mimo," in *2023 IEEE Future Networks World Forum (FNWF)*. IEEE, 2023, pp. 1–70.
- [5] W. M. Othman, A. A. Ateya, M. E. Nasr, A. Muthanna, M. ElAffendi, A. Koucheryavy, and A. A. Hamdi, "Key enabling technologies for 6g: The role of uavs, terahertz communication, and intelligent reconfigurable surfaces in shaping the future of wireless networks," *Journal of Sensor and Actuator Networks*, vol. 14, no. 2, p. 30, 2025.
- [6] A. A. Abba Ari, F. Samafou, A. Ndam Njoya, A. C. Djedouboum, M. Aboubakar, and A. Mohamadou, "Iot-5g and b5g/6g resource allocation and network slicing orchestration using learning algorithms," *IET Networks*, vol. 14, no. 1, p. e70002, 2025.
- [7] F. O. Catak, M. Kuzlu, H. Tang, E. Catak, and Y. Zhao, "Security hardening of intelligent reflecting surfaces against adversarial machine learning attacks," *IEEE Access*, vol. 10, pp. 100 267–100 275, 2022.
- [8] G. Kaur, V. Shrivastava, S. B. Khan, and A. Singh, "Applications of machine learning in strengthening 6g security," *Security and Privacy in 6G Communication Technology*, pp. 167–190, 2025.
- [9] K. Jain, P. Krishnan, P. Pachiyannan, L. Jaganathan, M. A. Khan, and Y. Li, "Toward smart 5g and 6g: Standardization of ai-native network architectures and semantic communication protocols," *IEEE Communications Standards Magazine*, 2025.
- [10] C. D. Alwis, O. Aouedi, J. Xu, S. Wang, Y. Siriwardhana, T. Hewa, E. Zeydan, C. Sandeepa, and M. Liyanage, "Federated learning for 6g security: A survey on threats, solutions and research directions," *IEEE Communications Surveys & Tutorials*, pp. 1–1, 2026.
- [11] J. Seo, F. O. Catak, C. Rong, K. Hong, and M. Kim, "Gc-fed: Gradient centralized federated learning with partial client participation," *Information Fusion*, p. 104148, 2026.
- [12] S. Hou, "Towards trustworthy intelligence: Safeguarding privacy and security in machine learning," Ph.D. dissertation, Hong Kong University of Science and Technology (Hong Kong), 2025.
- [13] A. K. Abasi, M. Aloqaily, and M. Guizani, "6g mmwave security advancements through federated learning and differential privacy," *IEEE Transactions on Network and Service Management*, vol. 22, no. 2, pp. 1911–1928, 2025.
- [14] M. Kumar and B. Mondal, "A brief review on quantum key distribution protocols," *Multimedia Tools and Applications*, vol. 84, no. 27, pp. 33 267–33 306, 2025.
- [15] K. Bonawitz and *et al.*, "Practical secure aggregation for privacy-preserving machine learning," in *Proceedings of the ACM Conference on Computer and Communications Security (CCS)*, 2017, pp. 1175–1191.
- [16] P. W. Shor and J. Preskill, "Simple proof of security of the bb84 quantum key distribution protocol," *Phys. Rev. Lett.*, vol. 85, pp. 441–444, Jul 2000. [Online]. Available: <https://link.aps.org/doi/10.1103/PhysRevLett.85.441>
- [17] F. O. Catak and M. Kuzlu, "A federated adversarial learning approach for robust spectrum sensing," in *Proceedings of the Mediterranean Conference on Embedded Computing (MECO)*, 2024, pp. 1–4.
- [18] F. Catak and M. Kuzlu, "A cryptographic federated learning-based channel estimation for next-generation networks," in *Proceedings of the IEEE Virtual Conference on Communications (VCC)*, 2023, pp. 92–97.
- [19] H.-K. Lo, M. Curty, and B. Qi, "Measurement-device-independent quantum key distribution," *Phys. Rev. Lett.*, vol. 108, p. 130503, Mar 2012. [Online]. Available: <https://link.aps.org/doi/10.1103/PhysRevLett.108.130503>
- [20] S. Zhou, L. Wang, L. Chen, Y. Wang, and K. Yuan, "Group verifiable secure aggregate federated learning based on secret sharing," *Scientific Reports*, vol. 15, no. 1, p. 9712, 2025.
- [21] C. Dong, J. Weng, M. Li, J.-N. Liu, Z. Liu, Y. Cheng, and S. Yu, "Privacy-preserving and byzantine-robust federated learning," *IEEE Transactions on Dependable and Secure Computing*, vol. 21, no. 2, pp. 889–904, 2023.